Spatio–Angular Microscopy

PhD Thesis

Martin Kielhorn

July 2012

Preface

<div align="right">M. K.</div>

Jena, Germany
July 2012

Contents

Contents

preface

add herbert gross to acknowledgements

hoffentlich kommen bessere prototypen nach mir

die programmierung verschiedenster hardware war ein wesentlicher aspekt ich habe mir ein beispiel an mikromanager genommen profitiert habe

ich hoffe dass diese arbeit einen grundstein legt. und dass jemand der damit beginnen will leichter den einstieg fidnet daher alle meine software auf github

die komplexitaet und stabilitaet wird zwar nicht erreicht das war aber nicht das ziel

ich wollte schnelles prototyping

1 Introduction

my device In this work I discuss a modification of a fluorescence microscope that minimizes the toxic effects of the excitation light.

phototoxicity In the following introductory chapter I describe what phototoxicity is and how it comes about. Then I give an example of how it influences biological observations in a developing *C. elegans* embryo and describe how this particular biological system can be used to evaluate and compare the phototoxicity of different microscopes.

cameras Later in this chapter I give an overview of image formation in the widefield microscope and I describe its principle limitations regarding resolution and depth discrimination. Furthermore I discuss the two most important current image detector technologies — electron multiplying charge-coupled devices (EMCCD) and scientifc complementary metal–oxide–semiconductor (sCMOS).

Regardless of whether it is the picture of earth captured by an orbiting satellite, the x-ray motion picture of a running dog or the time-lapse recording of a blooming flower. Images capture our imagination and they are a good starting point to develop new models and theories.

This is particularly true for microscopy. Only after people became aware of microorganisms by direct observation, medieval quack could finally be overcome and modern medicine based on the scientific method flourished instead.

Even today — with electron microscopes, magnetic resonance tomography and sequencing machines — optical microscopy still is an indispensable tool for research of living organisms.

labelling, switching Fluorescence microscopy is of particular importance: It enables the scientist to selectively label a particular type of molecule in living cells and observe how they perform their biological function.

Besides localizing molecules it is possible to measure physical quantities inside of the sample. There are, for example, fluorescent labels that report membrane potentials or viscosity inside of cells.

Finally, it is even possible to exert a controlling function with the excitation light: There are compounds that locally release chemicals when illuminated and there are genetically encoded ion channels that can be switched by light (?).

However, the excitation light introduces unnatural and potentially deleterious energy into the specimen. If the exogenous light harms the observed organism in any way, this effect is called phototoxicity.

There are a number of techniques that can reduce phototoxicity: Two photon excitation, controlled light exposure, selective plane illumination, highly inclined and laminated optical sheet, and oblique plane microscopy. I introduce them in chapter 2. These techniques have different pros and cons and not all are equally suited for a specific problem, e.g. selective plane illumination is very effective, but it needs two perpendicular lenses and can not be used for multiwell plates or to observe the liver of a living, adult mouse.

In this work I present an approach that makes use of modern display and camera technology. We only modify the microscope's illumination path, the space around objective lens and specimen remains as accessible as in any conventional wide-field microscope.

1.1 Phototoxicity in life sciences and the model organism C. elegans

⟨c:intro-phototoxicity⟩ The partner in our project who is responsible for decisions related to life sciences and biology is Institut Pasteur (Paris, FR). They work on infectious diseases.

In order to motivate the importance of phototoxicity, I would like to portray an elegant drug screening experiment which I have seen on one of my visits in Paris: An automatic microscope continuously images a cell culture in multiwell plates. These cells carry a pathogen. The pathogen, the nuclei of the cultured cells and the membranes of the cells are each stained with a different fluorophore. The cells in each well of the plates are exposed to a different chemical.

A chemical is considered a hit and will be investigated during further trials, when the time lapse images show that the culture cells stay healthy and the number of pathogens decrease. As neither people nor animals come to harm, this screening experiment is an impeccable method to systematically understand and hopefully heal certain diseases. However, this experiment doesn't work very well, if the excitation light — and not the drug — kills the pathogens. The effect of phototoxicity should therefore be minimized.

Now one would hardly develop a microscope and directly test it with dangerous pathogens. As part of our collaboration, the Institut Pasteur therefore developed a safe biological test system that is relatively easy to maintain (**?**) and allows to test the phototoxicity of various microscopes (**?**).

The basis of the system is the embryo of the organism *C. elegans*. These are small invertebrates. The adult form is approximately 1 mm long. Their anatomy and development are comparatively simple and have been well characterized (**??**).

We use embryos of a genetically modified strain[1] that expresses eGFP tagged histones (enhanced green fluorescent protein, excitation maximum 488 nm, emission maximum 509 nm). Histones are incorporated into the chromatin during cell divisions, i.e. the nuclei of our worms fluoresce green. The mother worm passes a sufficient amount of these proteins into the cytoplasm of the embryo. In the beginning of its development the embryo entirely relies on this reserve of histones. Only in a much later stage — certainly not during the first few hours, that we observe — it will form its own histones.

embryo example   Figure 1.1 compares time-lapse experiments on three different *C. elegans* embryos with varying excitation intensities.

reproducible devel-   The lineage tree of two developing *C. elegans* embryos is the same. With all
opment   other factors being equal, particularly if the temperature is constant at $21 \pm 1\,°C$, two different embryos will develop at the same speed from egg to fertile adult in three and a half days.

At the beginning of the experiment, embryos are removed from their mothers at an identical stage, before any cellular divisions have occured. Then a $z-$stack of the egg with 41 slices and one micron $z-$sampling is obtained every two minutes.

The columns in Figure 1.1 depict three different embryos whose development was imaged according to this protocol for two hours and 38 minutes with different excitation powers.

The figure displays the maximum intensity projections of the $z-$stacks. In order to make the cell nuclei visible in all images, I normalized the data to the same range. As can be guessed from the photon shot noise, the upper left image contains the least number of fluorescence photons, and the upper right the most.

An analysis of the time-lapse data show that one hour into the experiment the embryo with the highest excitation dose (right) has stopped developing and its fluorophores are strongly bleached. Some cells even turned apoptotic and went into programmed cell death.

After two hours and 38 minutes the experiment was stopped and the embryo

---

[1]Our strain has WormBase ID AZ212 (**?**).
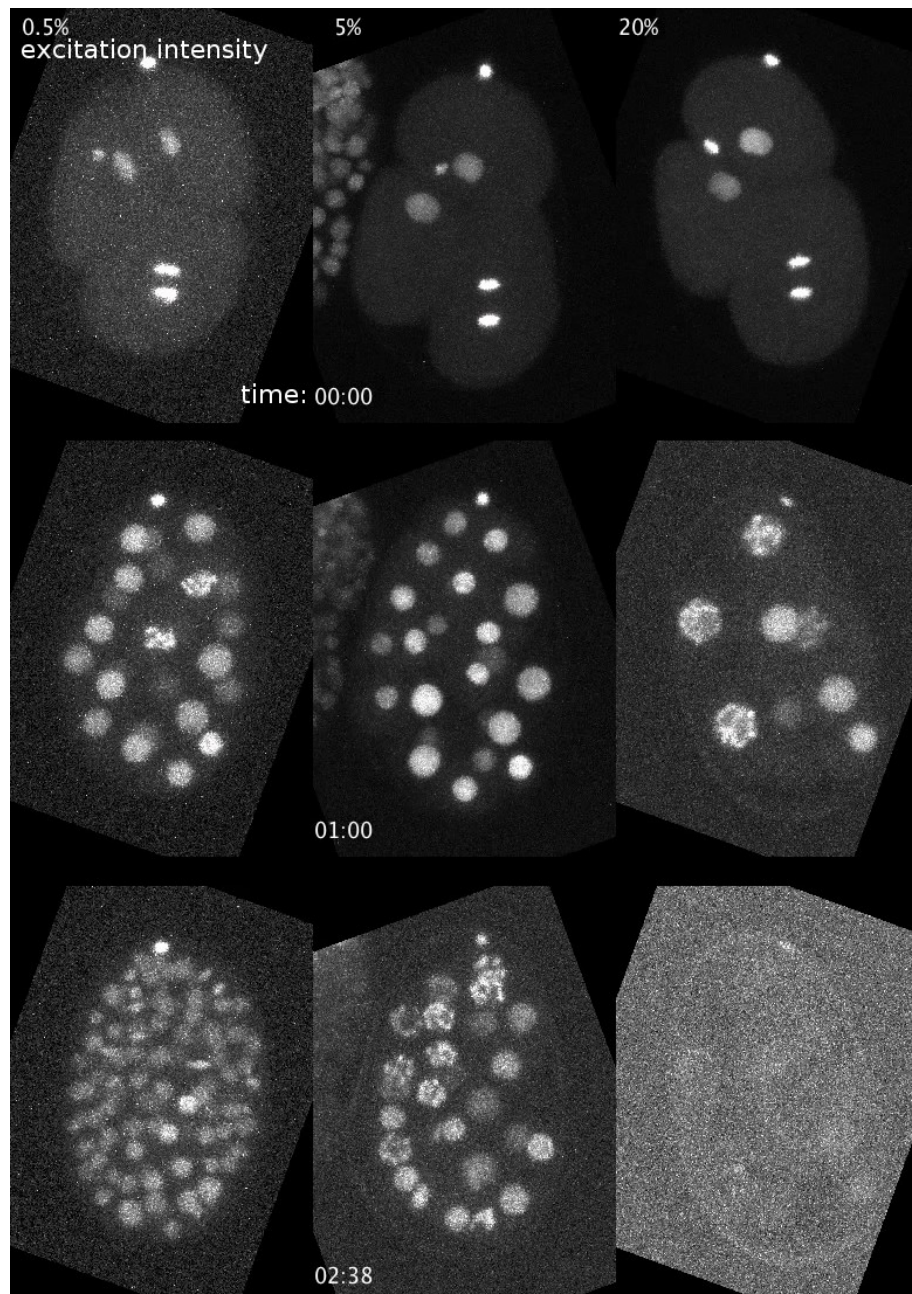
Figure 1.1: Phototoxic effects while imaging the embryonal development of three *C. elegans* embryos (strain AZ212, histone-2B tagged with eGFP) with different excitation intensities. The embryo with lowest excitation dosage (left) develops fastest. The embryo with the highest dosage (right) ceases development and nearly all fluorophores are bleached after the experiment. Images by J.-Y. Tinevez (Institut Pasteur, Paris, FR).

⟨fig:celegans-devel⟩

which was exposed to the lowest dose (left) has developed the largest number of cells. The middle embryo ceased developing while the right embryo died even

earlier and nearly all its fluorophores are bleached at the end of the experiment.

In Figure 1.2 I reproduce quantitative data from **?**. Each data point in this graph corresponds to a two hour time-lapse imaging experiment of a *C. elegans* embryo in a wide-field microscope. From a very low excitation up to a certain threshold dose the development isn't affected by the light and approximately 50 cells develop during the two hours.

For a dose above the threshold the development is slowed due to phototoxicity and the number of cells at the end of the experiment decreases.
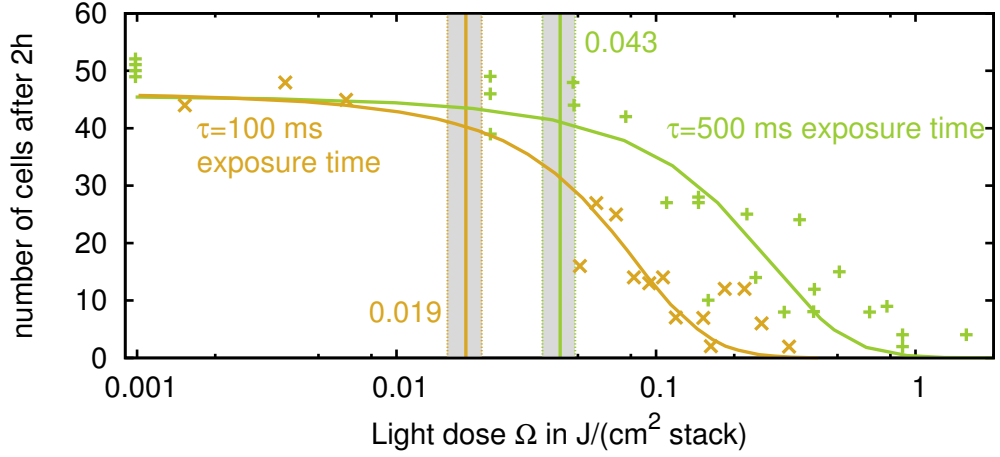
Figure 1.2: Longer exposure times are less phototoxic. Each data point corresponds to one embryo that developed under a particular excitation dose for two hours. The solid lines are sigmoidal fits to the data. Also indicated are the two phototoxicity thresholds given by the inflection point of the sigmoid and their 95% confidence intervals. This data was provided by J.-Y. Tinevez (Institut Pasteur, Paris, FR) and is also published in **?**.

worm-integration-time⟩

The orange data points in the diagram correspond to a per slice integration time τ of $100\,\text{ms}$ and for the green data the integration time is five times higher.

The dose Ω on the $x-$axis is calculated as

$$\Omega = \frac{\Phi_e n \tau}{A},$$

(1.1) {?}

with integration time τ, area A of the illuminated field, the number of slices $n = 41$ and radiant flux Φ_e of the excitation light, as measured in the pupil.

Naively one would assume that it shouldn't make any difference if the excitation light dose is administered with $100\,\text{ms}$ or $500\,\text{ms}$ exposures but these data show that a longer exposure time and low intensity are less phototoxic.

These results agree with an earlier study in tobacco plants (?). There is a threshold dose below which no phototoxicity can be detected, and the threshold decreases with light intensity. In the plants, Dixit and Cyr show that the damage is caused by reactive oxygen species and they explain the shift of the phototoxicity threshold by the limited capacity of the cells' scavenging system for those radicals. They also predict the existence of redox-sensitive checkpoints in the mitotic division cycle.

In summary this section describes how to measure phototoxicity with biological specimen. The next section gives an overview of the underlying photophysics and the rest of this work describes our attempt to build a microscope with reduced phototoxic footprint.

1.2 Basic photophysical principles of phototoxicity

Here I give a short overview of fluorescence of molecules in order to introduce the terms photobleaching and phototoxicity.

1.2.1 Absorption and emission of light

electronic transition A transition between a ground state S_0 to an excited state S_1 occurs, when a radiation field connects the two states. The connection is described by the transition dipole moment

wavelength range of fluorophores Photons with wavelengths below 200 nm have sufficient energy to ionize molecules. On the other side of the spectrum, a dye that absorbs in the near-infrared (> 700 nm) has a low-lying excited singlet state S_1 and potentially increased reactivity (?). Hence, most known stable and bright fluorophores absorb and emit in the wavelength range between 300 nm and 700 nm.

1.2.2 Depopulation pathways of excited states

energy levels The Jablonski diagram in Figure 1.3 summarizes information about the energy levels of a molecule and possible transition processes. If a molecule is in the ground state S_0 one of its outer electrons can be excited by absorbing a photon to the first excited singlet state S_1. If the photon has an even higher energy, the electron will go into the second excited singlet state S_2.

Transition from the ground state into higher electronic states than S_2 is not usual in commonly used fluorophores and wavelength range. Absorption of one
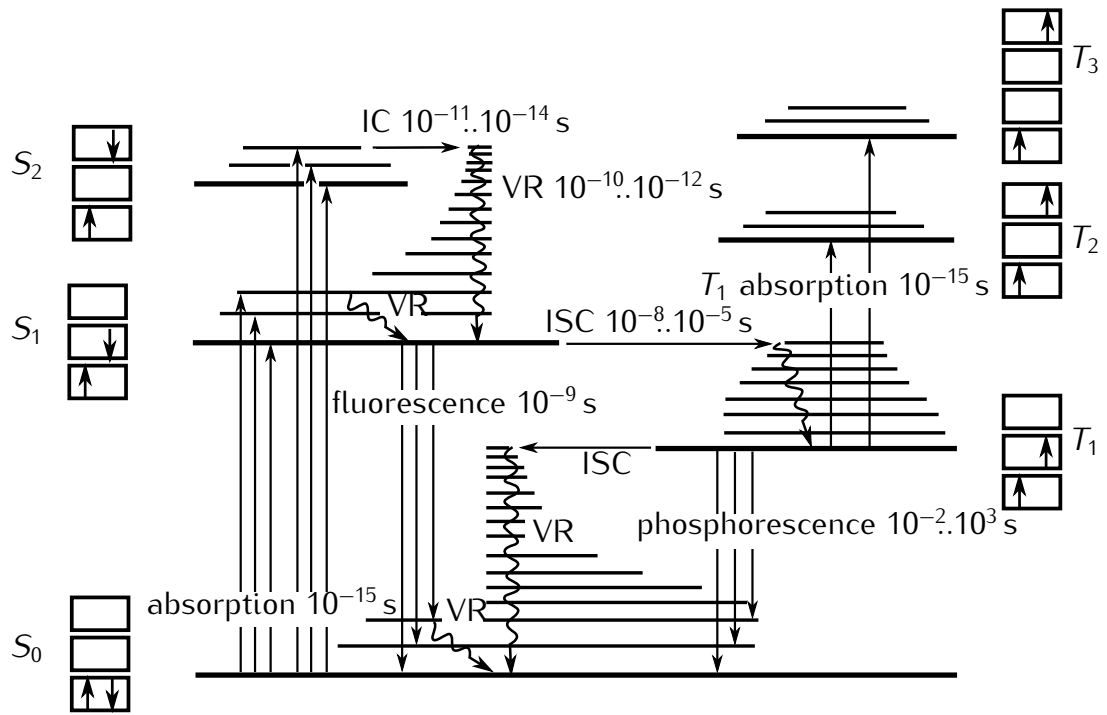
Figure 1.3: A typical energy level diagram. The boxes depict orbitals, up and down arrows symbolize the spin of the outer electrons. Fat lines represent electronic states. Thinner lines indicate vibro-rotational states. Various processes are shown with their typical time scales. VR = vibro-rotational relaxation, ISC = intersystem crossing, IC = internal conversion (inspired from ?).

⟨fig:flu-level⟩

photon doesn't change the spin of an electron and therefore the transition $S_0 \rightarrow T_1$ into the triplet state T_1 only occurs with very low probability.

Kasha's rule

solution rapidly damps vibrations

As described above, electronic excitation in general also leads to the excitation of a vibro-rotational nonequilibrium state (Franck-Condon state). In microscopy, fluorophores are often in solution, where they experience at least 10^{12} collisions per second. Inter- and intramolecular interactions bring the vibrations of the fluorophore molecule back to thermal equilibrium in a very short timescale (10^{-12} s). This is considerably less then the lifetime of the electronic excitation (few nanoseconds). Therefore spontaneous emission of a photon will occur from the vibrational ground state $S_{1,v_1=0}$ (*Kasha's rule*).

Stokes' shift

energy-loss = color change

During emission of a fluorescence photon a Franck-Condon state of the singlet

ground state S_0 is excited and returns into thermal equilibrium by vibro-rotational relaxation. Thus, some of the energy of the original excitation photon is lost as heat. The emitted fluorescence photon is red shifted compared to the excitation photon. Technically the *Stokes' shift* is defined as the difference of the wavenumbers of the fluorescence maximum and absorption maximum.

Intersystem crossing

spin flip forbidden

There is a small probability that the HOMO electron doesn't relax by internal conversion or emission of a fluorescence photon. Instead it flips its spin (due to spin–orbit coupling[2]). This process is called *intersystem crossing* and populates the first triplet state T_1. A transition into the ground state S_0 would need another spin-flip of the electron and is quite improbable. Therefore the triplet state has a long lifetime (up to several seconds). The radiative decay is called phosphorescence.

1.2.3 Photobleaching and phototoxicity

triplet reactive for long time

The prolonged lifetime of the triplet state T_1 increases the probability for the excited molecule to collide with a partner and react.

Figure 1.4: **left:** Molecular orbitals of the oxygen molecule. **right:** Molecular oxygen has the lowest energy in its triplet state $^3\Sigma$. Then the spins of the two π^*−electrons are parallel. Inspired from **?**.

⟨fig:oxygen⟩

oxygen likely reaction partner

The ground state of the oxygen molecule is a triplet state $^3O_2$, with two unpaired electrons of parallel spin in its π^*−orbitals[3] (see Figure 1.4). The triplet ground state and its abundance in typical microscope samples are the reasons why oxygen is so important when it comes to phototoxicity. If an oxygen molecule comes into physical contact with a T_1 fluorophore, e.g. ^{3}Chlorophyll*, the energy of the dye can be transferred to the oxygen by an electron exchange energy transfer mechanism in which the orbitals directly interact with each other (**?**, p. 438 and **?**):

$$^3O_2 + {}^3\text{Chlorophyll}^* \rightarrow {}^1O_2^* + {}^1\text{Chlorophyll} \qquad (1.2)\ \{?\}$$

---

[2] The probability of a spin flip is increased if heavier atoms are part of the molecule. E.g. while fluorescein has a triplet yield of 0.03, the triplet yield of eosin, a fluorescein derivative with four bromine substituents is 0.76 (**?**, p. 37).

[3] The antibonding molecular orbital π^* of molecular oxygen is constructed by linear combination of two atomic orbitals of oxygen.

This reaction is also known as triplet–triplet annihilation. There are two forms of singlet oxygen, that form in competition: The lower energy $^1\Delta$ and the short-lived, higher energy $^1\Sigma$ form ($T_{1/2} \sim 10^{-9}$ s), with spin orientations as depicted on the right of Figure 1.4. During the transition $^1\Sigma \rightarrow {}^1\Delta$ an infra-red photon with 1268 nm wavelength is emitted (**?**, p. 20).

effect of free radical

The resulting singlet oxygen $^1\Delta$ is very reactive. In a typical specimen it diffuses only a few tens of nanometre until it reacts with another molecule (**?**). When it reacts with the fluorophore, it can destroy it (photobleaching) also the singlet oxygen can damage the DNA of living creatures.

nature protects it-self

Plants have developed several protection mechanisms against being exposed to too much light. Within the cells they reorient and shift their chloroplasts in order to expose them to less light (**?**). However, they even have a molecular pro-tection mechanism: They transfer the energy of the chlorophyll onto carotenoid molecules and can prevent the hazardous *phototoxicity* effects of singlet oxygen (**?**).

methods preventing photobleaching

Nowadays many methods are known to reduce photobleaching: Substitute oxygen with noble gases or remove it enzymatically (**?**, p. 89), depopulate the triplet state by adding reducing as well as oxidizing agents to the solvent (**?**) or couple a triplet quencher directly to the fluorophore (**?**, p. 19). For fixed samples it helps to change the solvent or polymer.

hard to protect liv-ing sample

In living specimen these techniques may reduce photobleaching, but they can also have an effect on the biological system itself. Removing oxygen will quite certainly have a negative effect. In order to reduce phototoxicity it makes sense to think about the light management in the microscope.

1.3 Conventional microscopes

Microscopes that are in common use today do not optimally excite fluo-rophores within the specimen. In this section we outline how these mi-croscopes work. We explain how out-of-focus blur severely limits the per-formance of the wide field microscope. Then we discuss how confocal mi-croscopy improves the sectioning capability at the cost of increasing the phototoxic load on the specimen.

The basic building block of microscopes are lenses. A lens is a piece of glass with two polished spherical surfaces. Aspherical lenses also exist but are much harder to manufacture because of their lower symmetry. Light is slower in glass than

in air. The shape of a lens redirects photons and the thickness of the material can delay them. A lens ideally focuses a parallel beam of light into a spot on its focal plane. The distance between focal plane and the region where the rays start to converge is called focal length and denoted by f.

Figure 1.5: **a)** Schematic of a modern microscope. The sample is in the front focal plane of the objective. The detection tube lens TL1 forms a magnified image on the camera. **b)** Parallel laser epifluorescence excitation. The excitation tube lens focuses a laser into the back focal plane (BFP). The beam is reflected by a dichromatic beam splitter (BS) towards the objective. An extended area in the specimen is illuminated. Fluorescence light of lower wavelength returns through the objective, is transmitted through BS and forms an image on the camera. **c)** Confocal microscope. A pinhole PH2 is imaged as a diffraction limited spot into the specimen. Returning fluorescence light is only detected when it passes through an aligned pinhole PH1. This configuration rejects light that doesn't originate from the front focal plane (green) of the objective.

:widefield-microscope⟩

The uncoloured beam in Figure 1.5 a) represents rays that start from the intersection O of the optical axis and the front focal plane of the objective. The objective collects the rays and collimates them into a beam that is parallel to the optical axis. After traversing the tube length $f + f_{TL}$, the rays are focused by the detection tube lens TL1 on the intersection O' of its focal plane and the optical axis.

The blue beam corresponds to rays that start from an off–axis point P in the front focal plane of the objective. Behind the objective the blue beam is a parallel beam. However, the beam is tilted relative to the optical axis. The tube lens TL1 focuses the blue beam into a spot at P' on its focal plane.

The objective fulfils the Abbe sine condition – it is aplanatic. The microscope forms stigmatic[4] images of points from the front focal plane in the plane perpendicular to the optical axis, containing O' and P'. The plane with the images is called intermediate image plane. It is magnified by the factor M:

$$M = \frac{\overline{O'P'}}{\overline{OP}} = \frac{f_{TL}}{f}. \tag{1.3} \{?\}$$

In our microscope we use an objective with magnification $M = 63$. The focal

---

[4]An imaging system collects some of the rays, that leave an object and directs them towards the image. If all rays that leave an object point converge in the conjugate image point, then we call the image point stigmatic.

length of the tube lens is 164.5 mm for most Zeiss microscopes. Therefore the focal length of our objective is $f = 2.61$ mm.

Let's assume we have an opaque sample with just two small ($\varnothing < 120$ nm) holes with $2 \, \mu$m distance between them. We put this object into the front focal plane of the objective and position a camera on O'. When illuminating the mirror from the side opposite to the objective, the camera will show two spots with $126 \, \mu$m distance.

Note that Figure 1.5 depicts a *thin-lens model of a high numerical aperture objective* that fulfils Abbe's sine condition. A real objective contains in the order of ten coated lenses of different glass and crystalline materials. Their curvatures, positions and materials were all carefully chosen, taking into account manufacturing tolerances and wavelengths, so that the microscope behaves as the thin–lens model predicts. Diffraction at the periphery of the pupil in the back focal plane dictates the resolution, one can achieve inside of the sample.

It is quite possible that heating to 37 °C will ruin such a high–precision instrument. A related source of aberrations (departure of design performance) is the refractive index inside of the specimen. In Appendix ?? we describe a more complicated model that can predict the effect of embedding the sample in water (instead of immersion oil with the same refractive index as the glass).

1.3.1 Widefield epifluorescence microscope

Fluorescence photons are emitted in all directions, independent of the original illumination direction. Therefore it is possible and convenient to use the objective for excitation as well as detection. This mode of microscopy is called epifluorescence (Greek: $\varepsilon\pi\iota$; on, above). In this configuration usually only a small percentage of the excitation light returns due to diffraction or reflection. This simplifies the separation of fluorescence light from excitation light. Furthermore parts of opaque specimen can be imaged and it is beneficial that the illumination needs to be aligned only once.

The red beam in Figure 1.5 b) is a parallel laser. The excitation tube lens TL2 focuses the beam into the back focal plane (BFP) of the objective. The beam is reflected at a dichromatic beam splitter (BS). This is a glass plate that has been coated with dielectric layers. The refractive index, thickness and sequence of the layers are designed so that the excitation light is reflected towards the objective. Excitation light, that is scattered or reflected in the sample and returns through the objective is reflected towards the light source. However, lower energy flu-

orescence light returning from the objective is transmitted towards the camera. Behind the objective the beam is parallel and illuminates the specimen. The field of view is the demagnified diameter of the laser beam before TL2.

Non-uniformity due to coherent interference

Note that tiny dirt particles and coherent interference in laser beams can produce unwanted non-uniformities in the illumination. As a remedy the spatial coherence of the laser is sometimes reduced. Incoherent light emitting diodes, mercury or xenon arc lamps are often used instead of lasers. In the latter case a band pass filter selects the useful part of the spectrum of the excitation lamp upstream of the dichromatic beam splitter.

Out-of-focus blur

However, independent of the choice of the light source, the wide field microscope in epifluorescence configuration exposes many layers of the sample. This leads to fluorescence of out–of–focus fluorophores.

There are two reasons, why out–of–focus fluorophores give blurred images. Not even an ideal imaging system – a device that forms stigmatic images of all the points in one volume in another volume – would form sharp images on the camera plane. After all, the camera is just a plane and the object under observation is three dimensional.

Furthermore a microscope is far from being an ideal imaging system. In a microscope it is not possible to obtain a sharp image of a different slice of the object by changing the axial position of the camera behind the tube lens TL1 (??).

Deconvolution

When a stack of several slices of an object is obtained, it is possible to suppress the blurred part of each image in all the others. These algorithms (deconvolution) can improve the perceived quality of images in some stacks. However, there are two fundamental problems:

First the *missing cone problem* prevents focusing on a homogeneous fluorescent plane. Physics dictates that there is always a gap in the transfer function of the objective when the fluorescence process is linear and the objective collects only photons from one half space (see Figure 1.6). Not all spatial frequencies within the transfer function attenuate with defocus (?).

Figure 1.6: Schematic depicting $k_x k_z$−cross sections of the support of optical transfer function (see Appendix **??**) for microscope objectives with different collection angles. **left:** Objectives, that only collect light that is directed into one half space, have the missing cone problem. There, low spatial frequencies do not attenuate with defocus. **right:** Theoretical objective with larger collection angle and no missing cone.

⟨fig:missing-cone⟩

Second, even with ideal detectors there is photon shot noise in the image. In deconvolution algorithms the image of one slice is improved by subtracting blurred versions of the other slices. When the blurred intensity is large, its shot noise is high as well. Subtraction only increases noise and a faint in–focus image can be severely deteriorated by the noise of the out–of–focus light.

1.3.2 Confocal microscope

One way of addressing both problems of the wide field microscope is depicted in Figure 1.5 c). In the confocal microscope the whole field of view isn't illuminated simultaneously. The excitation tube lens TL2 collimates the light coming from a pinhole PH2 and illuminates the full back focal plane of the objective. In the front focal plane of the objective the red beam then converges to illuminate the smallest possible single spot. The spot size is defined by diffraction at periphery of the BFP. However, out–of–focus fluorophores are still being excited by the hour–glass shaped illumination.

The eponymous idea of the confocal microscope is to replace the camera with a pinhole PH1. This pinhole, if aligned carefully to the position of the image of the focused laser spot, has no influence on the light detected from in–focus fluorophores. However, an out–of–focus fluorophore that is defocused by Δz towards the objective will lead to a diverging beam (colorless) at the tube lens and will be imaged into a point behind the focal plane of the tube lens. The pinhole only transmits a part of the circle of confusion. Hence defocused fluorophores contribute less to the sensor signal.

An image of the in–focus specimen is obtained by scanning the pinholes PH1 and PH2 over the field of view and measuring intensity at each position individually. The optical removal of out–of–focus light prevents degradation of the signal by its shot noise and improves the point–spread function of the objective. The missing cone problem is fixed and the resolution improved by a factor of two. Note however, that information about out–of–focus fluorophores is lost which would be obtained in a wide field microscope with deconvolution. Therefore a wide field

microscope will give better results when a lot is known about the sample structure and this knowledge is fed into the deconvolution. E.g. the localization of sparse beads of specific size will be better in a wide field microscope.

The confocal microscope was invented in 1955 (**??**) to reduce the influence of scattering effects in neuron samples stained by Golgi's method. This invention preceded the laser and was unfortunately not put into practical use for biology until three decades later (**?**).

1.3.3 Phototoxicity in conventional microscopes

When imaging living specimen we should distinguish between useful and unnecessary excitation. Taking into account the detection capabilities of objective lenses we should maximize the ratio of in-focus to out-of-focus fluorescence. The epifluorescent wide field and confocal microscope surely do not represent an optimum in this regard.

The following chapter **??** will introduce other microscopy techniques that are more considerate of where to deposit excitation power within the specimen.

1.3.4 2-photon laser scanning fluorescence microscopy

?⟨sec:2-photon⟩? If the laser intensity in the focal spot of a confocal microscope is sufficiently high, then two infrared photons can be absorbed within $\sim 5\,\mathrm{fs}$ and excite the same electronic state.

In this regime, the fluorescence emission increases quadratically with laser intensity. This non-linearity confines the excitation volume to the vincinity of the focal plane (**?**). Fluorophores outside of this region are not excited. Therefore this method produces sectioned images by default and there is no need for a detection pinhole.

As an additional benefit infrared light is scattered less than visible light of half the wavelength. This increases penetration depth and image quality. Photodamage outside of the focal volume is unlikely and phototoxicity is much lower, compared to the single–photon confocal microscope, when $z-$stacks are acquired.

However, the phototoxicity within the focal volume is higher and techniques like ultramicroskopy (section **??**) with single–photon excitation are preferable, when low overall phototoxicity is a requirement.

1.4 Image detectors in wide field microscopy

Here we describe CCD sensors and their characteristics.

Charge-coupled devices are semiconductor devices that contain a 2D grid of capacitors, formed by at least three groups of electrodes (phases). Cycling the voltage on these electrodes allows to push charges, which has been accumulated under the capacitors (registers) into their neighbours. They turned out to be the ideal tool to move charges, produced by photon absorption in light sensitive diodes, across the substrate into read out logic.

Forty years of development lead to imaging devices with remarkable charge transfer efficiency, high quantum efficiency (up to 95% with back illumination) and very low dark currents. Until ten years ago the performance of CCD imagers in the low light regime was limited by the noise of the read out amplifier (a few electrons per pixel rms[5]).

Since the millenium we have electron multiplying CCD (EM-CCD) technology, which allows comparably good performance at low photon numbers (**??**) and moderate read out speeds (tens of MHz). EM-CCDs contain a row of additional registers in front of the read out circuit. There, one of the three phases is clocked with a much higher voltage (up to 40 V) then is needed purely for charge transfer ($\sim$ 6 V). The large electric fields cause charge carriers to be accelerated to sufficiently high velocities, so that additional carriers are generated by impact ionization. The charge multiplication chance per transfer is small ($\sim$ 1%) but by using several hundred registers a substantial gain in the number of charges can be achieved. In microscopy we usually work with gains of up to 300. Higher gains are possible but limit the dynamic range.

The charge amplification helps to push the read noise from $\sim$ 40 electrons rms to significantly below 1 electron rms — in effect creating a sensor limited only by the photon noise. However, the multiplicative nature of the gain leads to a perceived reduction in the quantum efficiency of the sensor (excess noise factor), i.e. an image with 100 photons/pixel without gain will look like the same image at only 50 photons/pixel with EM-gain (see Appendix **??**).

pixel in ccd ist passiv cmos ist aktiv

column parallel readout sony exmor

exmor r additionally back illuminated (only works for small sensors)

---

[5]root mean square

2 Methods of controlling illumination patterns

⟨sec:illum-patterns⟩

2.1 programmable array

?

3 The concept of spatio-angular microscopy

Here I introduce the spatio-angular microscope. First I motivate the concept of its illumination system using exemplary fluorophore distributions, that occur in typical specimen.

Then I describe some decisions we faced during the initial design phase concerning the arrangement of optical components. Furthermore, I position our method among known approaches of light control for microscopy. Of all published techniques for excitation illumination control, the light field microscope (?) comes closest to our approach. I explain differences between both techniques and discuss their respective pros and cons. I address the peculiarities and limitations of the hardware components in chapters 4 (optics) and 6 (micromirror based pupil plane SLM). Initially, the details would be detrimental to clarity.

It turns out, that the effective use of the spatio-angular microscope, requires more knowledge about the specimen than a conventional or a SPIM microscope (?). Ideally the distribution of refractive index and fluorophores in the specimen should be known. If these parameters were precisely known, there would be no need for an image in the first place. However, while imaging a known specimen, sufficiently good predictions of these parameters can often be made. The higher the accuracy of these prognoses, the greater the reduction in phototoxicity will be.

The computer-based selection of appropriate illumination masks requires the prediction, or at least an approximate estimation, of the three-dimensional distribution of light in the specimen.

In the last part of this chapter, I describe the computational control loop in our spatio-angular microscope and touch topics of image processing.

3.1 Motivation

In order to introduce the basic idea, underlying the spatio-angular microscope, first I consider the distribution of excitation light in the object of a conventional

fluorescence microscope: Figure 3.1 a) schematically illustrates the side view of the excitation beam path through objective lens and object in a confocal microscope. A parallel beam with a circular cross-section (this cross-section is not shown in the illustration) passes through the lens. The lens focuses the light in its focal plane.

Between lens and focal plane the light rays form a convergent circular cone. If refractive index variations in the object are negligible, the light distribution below the plane of focus forms a cone as well, due to symmetry. Assuming a non- or weakly absorbing specimen, the energy of the light in the circular cross-sections of the cone remains constant[1].

⟨sec:ray-valid⟩

The fluorescent bead (1), in the focus, would therefore be excited significantly more than the bead (2) outside the focal plane. Also shown is the light distribution in the intermediate image plane.

The image of the in-focus bead (1) is sharp, i.e. its emanating fluorescence light is concentrated on an area as small as possible and positioned exactly on the detection pinhole. Conversely, the image of the out-of-focus bead (2) is blurred and its fluorescence light is distributed over a large area.

While only a tiny proportion of the light emitted by the out-of-focus bead contributes to the detection signal of the confocal microscope—and therefore hardly affects the image quality, with respect to overall phototoxicity of the full confocal system—it would be better to prevent the excitation of the out-of-focus bead in the first place.

The scheme in Figure 3.1 b) demonstrates how the light cone would have to be manipulated in order to exclude the out-of-focus bead (4). The expected fluorescence image in the intermediate image plane then contains only information from the in-focus bead (3).

Viewed from the in-focus bead (3) the change in illumination corresponds to a restriction of the light angles. Such control can be exerted well through a mask in the other focal plane of the objective lens (also denoted back focal plane or pupil plane).

---

[1]The ray-model is valid in large parts of Figure 3.1 a), but not everywhere. The Law of Malus–Lupin states that rays and wavefronts are equivalent as long as rays do not intersect (caustic), or (FIXME formulas?) a strong intensity gradient occurs. Thus the ray-model is valid almost everywhere in the cone, except for a region with a distance of a few wavelengths to the edge, and the focus itself. While the wave-optical treatment of these areas is possible, it is computationally much more expensive than ray tracing. Wave-optical effects either lead to blurring in a length scale of a few wavelengths or intensity fluctuations due to interference. If necessary, we can use heuristics to find an upper bound for the local intensity from ray tracing results. For this reason we exclusively employ the ray-model in this work.
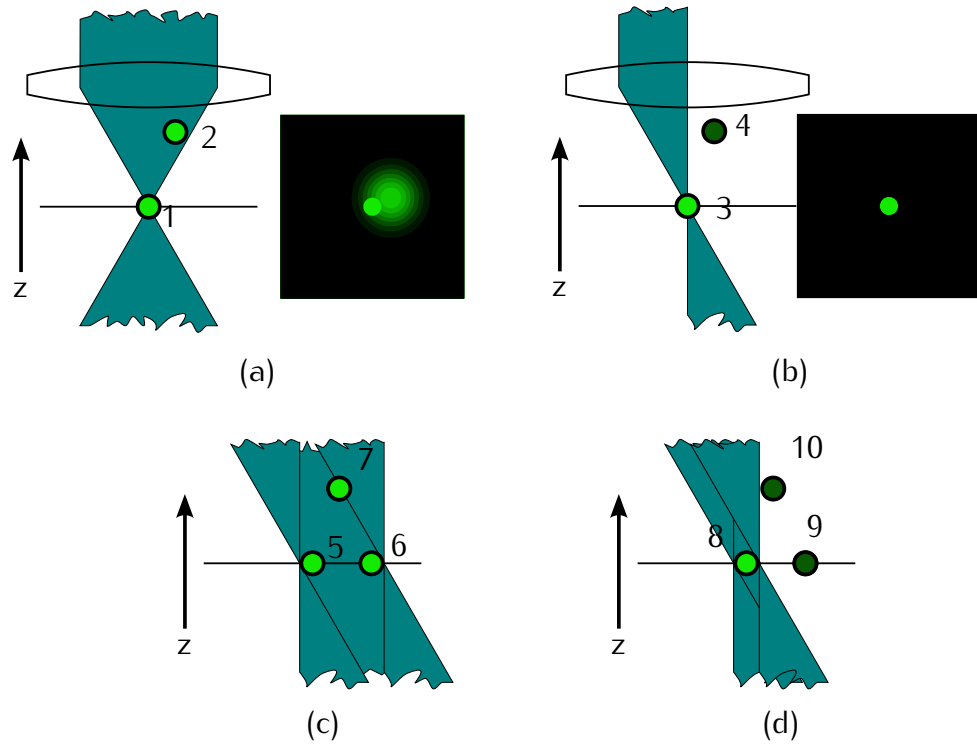
Figure 3.1: **(a)** Two fluorescent beads are illuminated by all angles that the objective can deliver. The sharp image of the in-focus bead is deteriorated by blurry fluorescence of the out-of-focus bead (2). **(b)** Angular control allows selective illumination of the in-focus bead (3), and results in a better image on the camera. **(c)** Angular control, however, is insufficient, when an extended in-focus area is illuminated. **(d)** Then, simultaneous spatial and angular control allows sequential excitation of the in-focus beads, while excluding the out-of-focus bead (10).

⟨fig:hourglass-all⟩

Thus I have shown that it is useful and possible to equip a confocal microscope with angular control. However, in our project we set out to to build a wide field microscope in order to benefit from the speed and quantum efficiency of modern cameras.

I now turn to the task of bringing angular control to the wide field microscope. Figure 3.1 c) shows a configuration of the specimen with two in-focus beads (5) and (6), and one out-of-focus bead (7). The angular illumination control is ineffective for this arrangement of beads. If both in-focus beads, (5) and (6), are exposed simultaneously, i.e. an extended light source illuminates the entire field, then the out-of-focus bead (7) is always excited.

Only by separate illumination of the in-focus beads (8) and (9), as shown in Figure 3.1 d), angular control regains its function. For this reason a wide field system with angular control, using a mask in the pupil, requires an additional

mask in the field. Therefore, we call our method spatio-angular microscopy. "Spatial" refers to the illumination control in the field and "angular" refers to the control in the pupil plane.
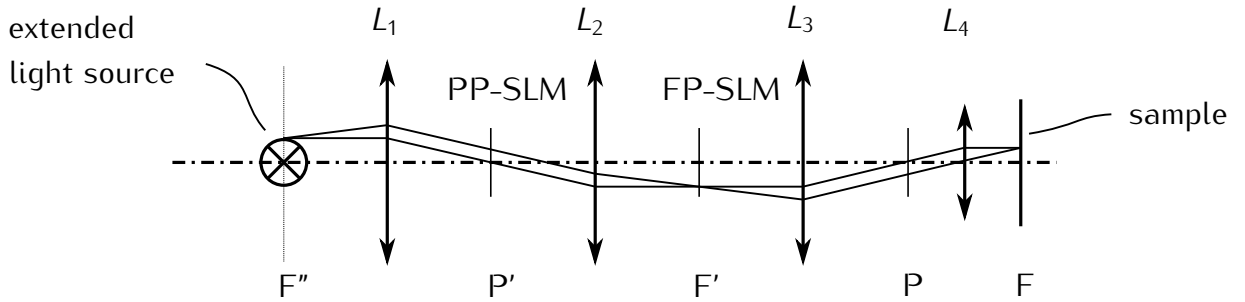

Figure 3.2: Simplified schematic of the illumination system in our spatio-angular microscope. A homogeneous extended light source delivers light from the left. It is imaged by lenses L_1 and L_2 into the intermediate image F'. Then the tubelens L_3 and the objective L_4 form an image of F' in the sample plane F. We use two spatial light modulators (SLM) to control the spatial and angular light distribution in the specimen—the focal plane SLM in F', and the pupil plane SLM in P'.

⟨fig:memi-simple⟩

Figure 3.2 shows the optical path through our prototype in a greatly simplified form. From the left side, an extended light source illuminates the system. A sequence of telecentric lenses L_1, L_2, L_3 and the objective lens L_4 image the light source from F" into the front focal plane (indicated by F, for field). The etendue $\mathcal{E} = \frac{\pi}{4}(D_{\text{field}} \text{NA})^2$ — also called information capacity, light gathering capacity or space–bandwidth product; its value is related to the number of point spread functions that can be resolved in the field (FIXME check definitions, put formula somewhere else, area of the light distribution convolved with the solid angle)) — of the light source must be large enough to simultaneously fill both, the pupil P as well as the field F.

In each of the two planes P' and F' we place a spatial light modulator (SLM) that allows to control the intensity of the transmitted light.

Looking at the scheme in Figure 3.2, one might argue that we could save a lens, if we placed the pupil plane SLM into P instead of P'. There are three reasons why this is neither possible, nor beneficial: First, the pupil of modern high-performance objective lenses is typically not accessible. Second, the detection path for fluorescent light should contain as few optical components as possible and we can definitely not afford it to be blocked by a SLM. Third, the two masks induce non-linear, and therefore difficult to predict, filtering of spatial frequencies. An analysis requires consideration of partial spatial coherence, but it should be

clear (FIXME) that only the downstream SLM will always deliver a good image, mostly independent of the state of the SLM upstream.

Considering the fact that the image of the focal plane SLM is most important to us, we decided to place it downstream of the pupil plane SLM. The focal plane SLM may disturb the image of the pupil plane SLM in P, but we can always produce very fine, high-contrast structures in the sample F.

The abiltity to achieve high resolution in the field is the main difference between our approach and Levoys light field microscope. In the light field microscope, the density of the microlenses noticeably limits the resolution. As opposed to our system, the light field microscope allows to control the angle of incidence in all field positions independently. But, additionally to the reduced focal plane resolution, this requires a single high-resolution SLM with a comparatively low refresh rate. We use two small SLMs, which can each achieve 1 kHz frame rate and enable interesting experiments, e.g. optogenetic control of neuron activities.

Furthermore, structured illumination with high resolution patterns allows us to circumvent the missing cone problem of the widefield microscope. Later I will show that depth discrimination improves with higher resolution patterns (FIXME ref).

3.2 An imaging protocol with spatio-angular illumination control

3.2.1 Description of an exemplary biological specimen

I now refer to the *C. elegans* test sample for phototoxicity that I introduced in section 1.1. As I will discuss in later (FIXME) chapters, so far I did not reach the point of being able to image the development of a real embryo. Key problems are the low light throughput of the illumination system and the length of time necessary to update images on the focal plane display. Nevertheless, I always kept this example in mind while I was developing the control software for our microscope.

During the first few hours, the embryo develops confined within the constant volume of its egg, which has an ellipsoidal shape, extends 40 to 60 microns and can be readily observed using a 63× objective lens. Cell divisions occur every few minutes. During development the nuclei get smaller and more dense. In order to track the fate of all individual cells it is sufficient, to capture one stack

per minute with 41 layers and a z−step of 1 micron.

3.2.2 Preparation of living embryo samples

For an experiment a hermaphrodite worm is cut and the embryos are placed on an agarose pad, so that they stay immobile during imaging. This procedure is explained[2] in **?**. Of these embryos, the experimenter chooses a young specimen, that has not yet divided. We avoid to use fluorescence excitation for this step. The undivided embryos can be distinguished using the less phototoxic differential interfernce contrast (DIC) imaging mode.

3.2.3 Sectioning through structured illumination

To get an estimate of the initial distribution of the fluorophores in the embryo I obtain the very first stack with structured illumination and no angular control. I use this method to avoid the missing cone problem of the widefield microscope. Perhaps for our particular task of finding the position of one nucleus within the egg, widefield images would be just sufficient. However, for our spatio-angular method, knowledge about the fluorophore distribution is very important and therefore we built our microscope such that we can obtain optical sections.

We compared conventional structured illumination using max−min (FIXME) reconstruction with laser and LED illumination. Although LED illumination resulted in excellent optical sections, the reconstruction of laser illuminated images contained artifacts.

– (FIXME muss das vielleicht in appendix?) In einem ersten Entwicklungsschritt, bevor InVision uns den Prototyp fuer das spatio-angulare Mikroskop zur Verfuegung stellte, setzten wir einen SLM in die Zwischenbildebene. Auf dem SLM wurden vier Streifenmuster angezeigt und Wir verglichen einen 70mW 473nm DPSS laser mit 470nm LED Beleuchtung (CoolLED).

Therefore, we decided to implement HiLo (see Appendix FIXME). With this algorithm, we obtain artifact-free optical sections, regardless of the illumination source. As another advantage the HiLo method increases acquisition speed, as only two raw images per slice are necessary.

wir haben artefakte in der max-min rekonstruktion beobachtet, wenn wir ein grobes streifenmuster (8 forthdd slm pixel periode) mit laser beleuchtet haben

---

[2]Note that **?** describes an improvement of this protocol that prevents squeezing the embryos too much.

– irgendwann hat rainer das erklaert aber ich kann mich nicht mehr dran erinnern aber es waere cool, wenn ich die story bringen koennte

– grobes gitter heisst im amplitudenbild: einige ordnungen (nicht nur 3) gehen durch die bfp

– irgendwie kam es dadurch im intensitaetsbild zu einigen hoehere ordnungstermen

– bei LED (extended source) werden die weggemittelt, bei laser nicht

– ein bisschen kopfzerbrechen bereitet mir noch der bias

– im paper habe ich das nicht verstanden [2011 mertz Optically sectioned in vivo imaging with speckle illumination HiLo microscopy]

– aber ich habe ihr java imagej plugin decompiliert bekommen und koennte versuchen ihre implementierung zu verstehen (andererseits ist mir das jetzt ziemlich egal)

– unter equation 10: The first two terms are variance contributions of shot noise. Filtering has the effect of reducing noise variance and is taken into account with the integral term. This bias must thus be subtracted from σ^2 prior to the evaluation of C. We have also not considered the effects of pixelation in the CCD camera. If the pixel size is non-negligible ..

3.2.4 Computer model for the integration of a priori knowledge about the biological events

Given an initial measurement of the fluorophore distribution of the embryo, I employ a computational algorithm to find good illumination conditions for subsequent stack acquisitions. An important requirement is that the computer can estimate, which areas of the sample should be protected from illumination.

For our test system, the *C. elegans* embryo, it is a promising approach to represent its three-dimensional fluorophore distribution by a simple model: Spheres encompassing the nuclei, indicate regions with fluorophores. When in focus, the spheres are the source of useful, informative fluorescence signal, but should be protected against exposure when out of focus.

As I mentioned earlier, there are also unused histones with fluorophores outside of the nuclei. The images reveal that they occur in the cytoplasm at a much lower concentration than in the nuclei. Fluorophores in the cytoplasm have a smaller phototoxic effect, because any radicals they produce are much less likely to reach the DNA and therefore inflict substantially less damage. In the following my goal is to protect only out-of-focus nuclei from exposure. The regions in between are

used to bring the light in.

During observation, the nuclei, i.e. the centers of the spheres, move slowly within the embryo. For small periods of time we can describe this movement using a vector field of growth velocities.

A cell division announces itself by a change of the fluorophore distribution of the nucleus due to chromatin condensation and spindle formation. Therefore, whenever the computer detects such changes in the images, in one of the following time steps an additional sphere should be introduced to account for the new daughter cell.

So far I have only implemented a simple algorithm, to convert a time series of image volumes from a confocal microscope into a sphere model (FIXME difference of Gaussians and radius determination blob paper). One of our project partners (Jean–Yves Tinevez, http://fiji.sc/wiki/index.php/TrackMate) developed a more sophisticated plug–in for ImageJ, that provides the lineage tree and snapshots of the developing cells (see Figure 3.3). Before our microscope can be used
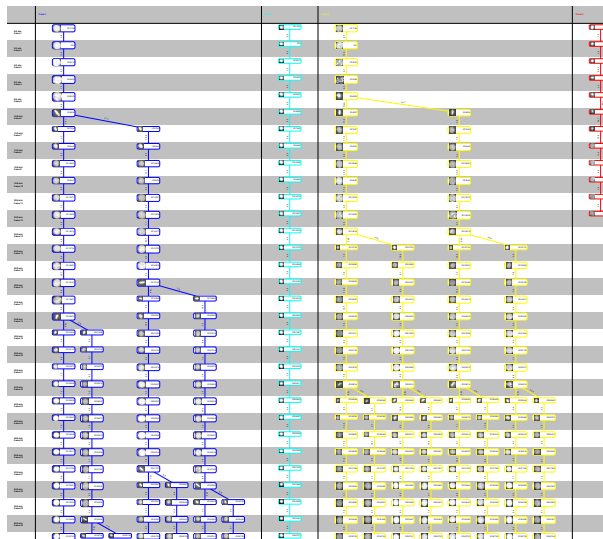
Figure 3.3: A detail of a lineage tree visualized in TrackScheme. An image of each nucleus is shown in each time step. Note how the elongated structure before cell division events. (FIXME ask jean–yves if i can use this, add time axis)

⟨fig:trackmate⟩

for our biological problem, the computer model has to be extended so that it reliably tracks the movement of nuclei. Overlooking any nucleus would prevent this nucleus from being imaged in later acquisitions and would be a setback for the experiment. Estimating the vector field of growth velocities helps to track nuclei more robustly and allows to predict their positions for the next exposure.

Unfortunately, currently we have not implemented programs that would fulfill the requirements for imaging a developing embryo. However, in the following text I assume that the described position predictions were available and I discuss how I determine masks for the focal plane and pupil plane SLM.

?

TODO FIXME Bernhard Kauslers work is nice `http://archiv.ub.uni-heidelberg.de/vo` Live-cell microscopy image analysis for the study of zebrafish embryogenesis `http://hci.iwr.uni-heidelberg.de/publications/mip/techrep/kausler_12_discrete.` A Discrete Chain Graph Model for 3d+t Cell Tracking with High Misdetection Robustness

(FIXME read this)

3.2.5 Illumination optimization by means of raytracing

I now discuss a method to find both SLM masks for image acquisitions with minimal phototoxicity. First I define a mask for the focal plane SLM:

From the predicted arrangement of spheres we select in-focus nuclei by intersecting the model with a planar surface. I then define focal plane SLM masks to selectively illuminate each of the in-focus nuclei, by drawing a bright disk in the appropriate position.

Based on such a mask, we can determine which angles can illuminate the in-focus target nucleus, without exposing out-of-focus nuclei.

As we already explained at the beginning of this chapter on page 23, ray-optical theory suffices to describe the light distribution within the sample.

I connect the periphery of an out-of-focus nucleus with a point inside the in-focus target. This defines a circular cone of rays, that are propagated through the objective lens. Their intersection with the pupil plane results in a figure that still very much resembles a circle—I found that already seven rays lead to good representation of its perimeter. I compute these figures for every out-of-focus nucleus and for a few in-focus targets points within the bright areas of the focal plane pattern. In this manner I construct the desired mask for the pupil plane SLM.

In order to trace the rays into the pupil, I need the design parameters of the objective lens (vertex position, curvature and material for all surfaces). Unfortunately, these rarely are publicly available for high-performance objective lenses. Nevertheless, in chapter (FIXME) I use a simpler model of the objective lens, that requires only three parameters: focal length, refractive index of the immersion

medium and numerical aperture. These are always known.

Additionally, I have adapted the model for non–index–matched embedding of the specimen. This problem occurs, when the embryo is illuminated with an oil immersion objective, using HILO (FIXME ref). It should be noted, however, that good image quality of the embryo can only be achieved with an objective lens that has the same immersion index as the embryo. Otherwise data from 20 microns within the sample will be severely deteriorated by spherical aberrations.

4 Device 1: prototype for spatio-angular illumination

In the preceding chapter I showed the underlying concept of our cmmore specific problems spatio-angular microscope. Here I discuss additional details that are important for the practical implementation.

I explain the beam path, electronic synchronization of the displays with other components and an algorithm to transform the coordinate system of the camera pixels into the coordinate system of the focal plane SLM.

The pupil plane SLM was specifically developed for our project by cmMMA details later our partner Fraunhofer IPMS (Dresden, DE). Therefore I dedicate chapter 6 on page 42 to this device.

4.1 Description of the optical components

So far we have only shown the beam path for transmissive displays (in Figure 3.2). Such SLM only have a very low transmission in practice. Therefore we use reflective displays in our prototype.

In Figure 4.1 I adjusted the beam path accordingly. This schematic also depicts the optics we use to adapt light from the laser to fill the etendue of our system. The light source enters the system from the bottom left. The optic components are color corrected and have anti-reflex coating for wavelengths in the range from 400 nm to 700 nm.

The system successively illuminates the pupil plane SLM—a grayscale micromirror array developed by our project partner Fraunhofer IPMS Dresden—and the focal plane SLM, a commercial binary liquid crystal on silicon display.

I gathered some of the following details from the documents that were created during the development of our prototype and are classified as confidential. I have summarized the key decisions here and the relevant project partners have agreed to the publication (FIXME not finished).
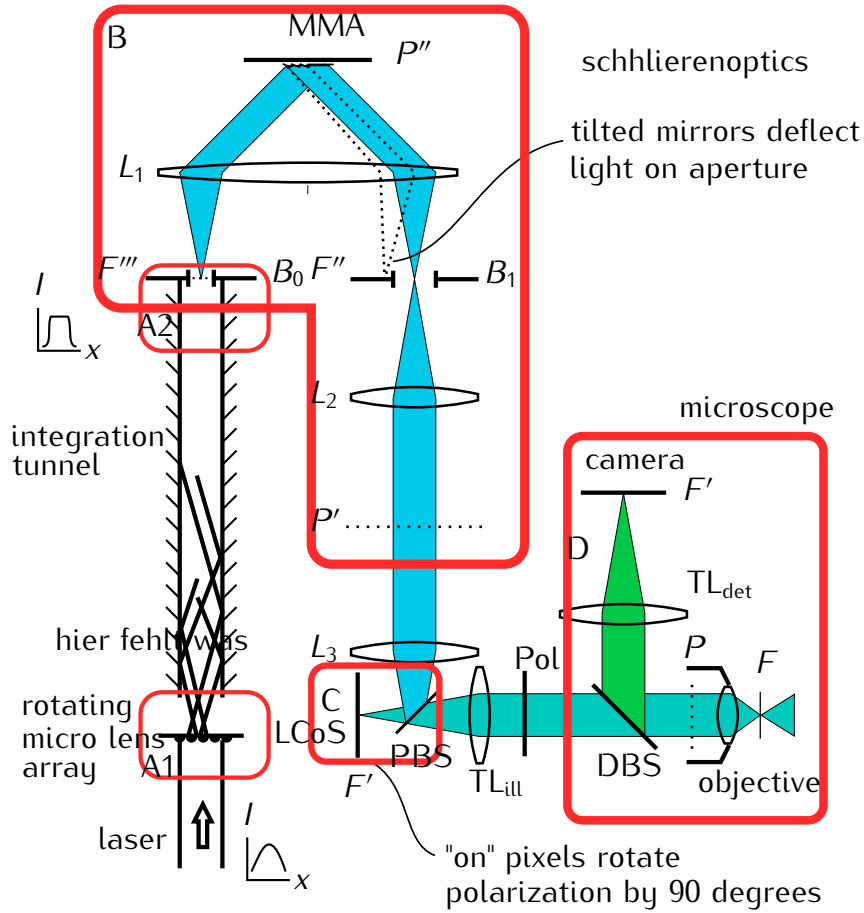
Figure 4.1: Schematic of the light path through our microscope. Laser light enters from the lower left, is scrambled and homogenized to illuminate the pupil plane SLM in P″ and the focal plane SLM in F′. *F* is the field plane in the sample and its primed versions are conjugated planes. *P* is the pupil of the objective. B_0 and B_1 are adjustable circular apertures. PBS is a polarizing beam splitter. DBS is a dichromatic beam splitter. The red boxes deliminate subsystems of the illumination system: **A:** light scrambling and homogenization, **B:** Fourier-optical filter to provide intensity modulating pupil plane SLM. **C:** Polarization based intensity modulator as focal plane SLM. **D:** Wide-field fluorescence microscope with detection path. (FIXME finish diagram, don't use B twice)

⟨fig:memi-real⟩

4.1.1 Ensuring homogeneous illumination

A quantitative evaluation of our experiments (FIXME ref sec:results) with different illumination patterns is simplified when both pupil plane SLM and focal plane SLM are uniformly illuminated.

We use either a laser[1] or an light emitting diode (LED) as the light source in our experiments. Below we discuss optical measures that attain homogeneity of the illumination of both displays.

The LED[2] we use has a large active area. Due to etendue mismatch a relatively large amount of its produced light will never reach the sample. But it is easy to achieve a homogeneous illumination. Moreover, the LED can be quickly switched on and off electronically [3].

Unlike an LED, a laser delivers light of considerably higher spectral radiance ($W/(sr\,m^2 m)$). Thus it is in principle possible to use the laser as a highly efficient light source for our system. Unfortunately, the high spectral and spatial coherence of a laser often lead to high–contrast fluctuations of the irradiance and we have to compensate for this by time averaging.

When using the Laser, we send its parallel Gaussian beam into a bundle[4] of randomly distributed fibers. This randomizes the light distribution at the bundle output and also broadens the illumination angles.

A relay system (A1) images the circular output of the fiber bundle onto the entrance of a light pipe. This relay system contains a rotating microlens array[5]. It is driven by a motor with the axis of rotation being diplaced from the optical axis. This time-varying element allows to reduce speckle.

Both, the fiber bundle and microlens array, increase the etendue of the laser illumination to the optimum value, which is given by one of our SLM as discussed below in ?? (FIXME ref).

The light pipe is a hollow mirror–integrator tunnel with quadratic cross–section and depicted in Figure 4.2. The mixing effect of the tunnel can be understood by considering the irradiance in the plane of the tunnel output as it would occur

---

[1] Lasever LSR473H, diode–pumped solid state laser, output power 600mW, $\lambda = 473\,nm$

[2] Huey Jann HPB8-48KBD, wavelength $(463 \pm 1)\,nm$, brightness $35\,lm$, view angle 120°, FIXME TODO: Flaeche messen

[3] The DPSS Laser doesn't allow fast direct electronic switching at full power. We have to use an acousto-optic modulator connected with the additional expense of its optical alignment (FIXME siehe spaetere ref section).

[4] Fiber bundle with circular cross-section (Loptek, Berlin, DE), 1.1 mm diameter and 2 m length. The beam broadening is 3° and increases, when the bundle is bent (?).

[5] Array of cross–oriented cylindrical lenses on both sides with a pitch of 0.5 mm resulting in an effective focal length of 6.9 mm (LIMO, Dortmund, DE).

without tunnel.

Drawing the outline of the square cross-section into this irradiance map selects the light that directly reaches this plane. Surrounding this outline with the four squares that touch its edges selects the light that will reach the output plane after one reflection. The irradiance maps from neighbouring squares are mirrored and added to the direct illumination. Depending on the numerical aperture of the input light, more reflections may occur — resulting in the addition of irradiance from next–nearest–neighbours and so forth.

This improves the uniformity of the light distribution in the output plane without altering the numerical aperture of the light. The more subregions are superimposed, the better will be the uniformity. Assuming N subregions were overlaid and their contributions were statistically independent, then according to the central limit theorem the standard deviation of the irradiance is proportional to $1/\sqrt{N}$ (?).

However, we also align the source distribution to be rotationally symmetric about the optical axis and obtain an even more uniform output than this prediction because positive and negative slopes from different subregions compensate in the superposition (also ?).

In our system the side length of the cross-section of the tunnel is 2.5 mm and its length of 250 mm ensures enough reflections for homogeneous illumination. A relay system magnifies the tunnel output to 4 mm × 4 mm in the plane F‴.

We thought about using the output of the tunnel directly, without the additional relais system, but then the length of the tunnel would have been prohibitively long.

Regarding the two relay systems the optical designer at In–Vision commented (FIXME ref D8.9) that these have not been optimized for prefect imaging but for the transport of the homogeneous light distribution. The system A1 at the tunnel entrance has to transfer the illumination from the round fiber end to the square tunnel entrance. The engineer designed a good quality system with only two lenses (and the microlens array). At the other end (A2 in Figure 4.1) five elements carry the light from the tunnel exit into F‴.

During the planning phase we also considered a homogenization design based on a fly's eye condensor (two consecutive microlens arrays). According to simulations performed by In–Vision, this, however, would have been more difficult to adjust than the tunnel. In particular the system would have been more dependent on illumination wavelength.

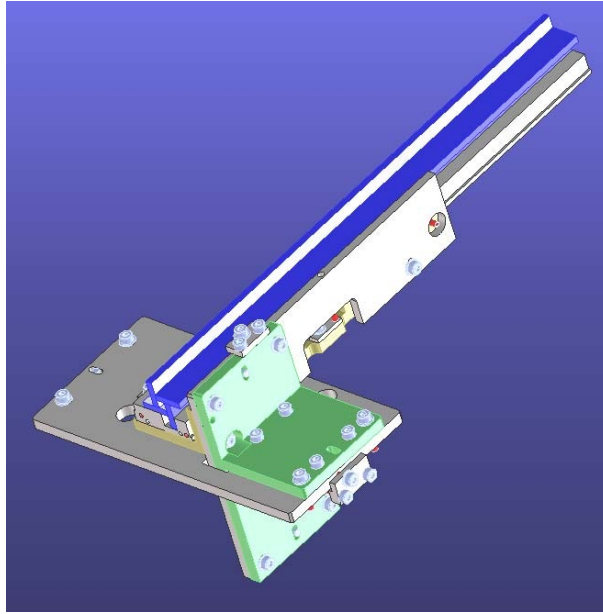In summary the following points are important in order to achieve homogeneous

Figure 4.2: Hollow mirror–integrator tunnel with a quadratic cross section of 2.5 mm side length and 250 mm length.

⟨fig:integrator-rod⟩

illumination of focal and pupil plane with the tunnel:

- The image of the end of the bundle should properly cover the tunnel entrance. Especially the corners of the tunnel should not be darker than the center. Inhomogeneous illumination at the tunnel entrance leads to inhomogeneous illumination of the pupil plane SLM.

- The end of the fibre bundle must be adjusted in four axes (centering and angle).

- The focal length of the microlenses should be chosen shorter than predicted by pure etendue calculation. In order to compensate inevitably occuring microchipping on the edges of the cemented glass mirrors.

4.1.2 Fourier optical filter for contrast generation on pupil plane SLM

The micromirror array, which we use as a pupil plane SLM consists of torsion mirrors that modulate the phase of the light (for a more detailed description see ref FIXME). In order to modulate the intensity we use the Fourier filter shown in Figure 4.1 B.

The lens L1 has two purposes: First, it images the field mask B0 into the field stop B1. Second, the plane P″ with the phase SLM is imaged to infinity.

With undeflected micromirrors, the SLM has no signifcant effect and works like a plane mirror. Both planes F″ and P′ are then homogeneously illuminated.

If the left half of the micromirrors are tilted, then they direct the light along the dashed line in Figure 4.1. This light is absorbed by the field stop B1 and therefore missing in P′, i.e. the right side in P′ is dark. The total radiant flux (W) through the beam stop in F″ decreases while the transmitted irradiance (W/m^2) remains homogeneous.

In the real system, the lens L1 consists of four elements.

4.1.3 Relay optics between pupil plane and focal plane SLM

The lenses L2 and L3 form a double-telecentric relay system with magnification 2 and image F″ onto the focal plane SLM in F′. At the same time these lenses make sure that the pupil plane SLM is imaged to infinity.

The relay system ensures that the pixels of the focal plane SLM are at the resolution limit, while the pupil plane SLM fills the pupil.

In addition, the relay system enables a simpler mechanical realization and good contrast. It would already be difficult to accommodate the focal plane SLM and polarization beam splitter in F″ — including an adjustable aperture would probably not be feasible at all.

4.1.4 Contrast generation on focal plane SLM using polarization

The SLM we use to control the focal plane illumination is a ferroelectric liquid crystal on silicon device (ForthDD WXGA R3, UK). Depending on if a pixel is off or om, the returning light either retains the polarization of the input light or rotates it by 90 degrees.

From this, a polarization beam splitter generates a binary intensity contrast (see Figure 4.1 C).

We opted for a wire-grid polarization beam splitter (Moxtek PBF02C, Orem, UT, US) because they ensure a high enough optical quality, good contrast and the plate causess less back reflections than a beam splitter cube.

– ignacio moreno 2009 operational modes of a ferroelectric lcos (FIXME)

The s-polarized component of the incoming light is reflected towards the SLM. Active pixels of the SLM rotate the polarization of light by 90 degrees and then passes through the beam splitter as p-polarization in the direction of the microscope. There is a supplementary cleanup analyzer in the beam path.

It would also be conceivable to arrange SLM and beam splitter differently, so that the light coming from the SLM is *reflected* towards microscope. In this case, however, unwanted bending of the beam splitter's surface will deteriorate the image quality of the focal plane SLM. Therefore, we use the beam splitter in transmission.

The beam splitter plate makes the overall optics slightly assymmetric and thus induces mainly astigmatism and lateral color (ref FIXME D8.9). The plate is thin enough (thickness 0.7 mm), so that the design remains diffraction limited.
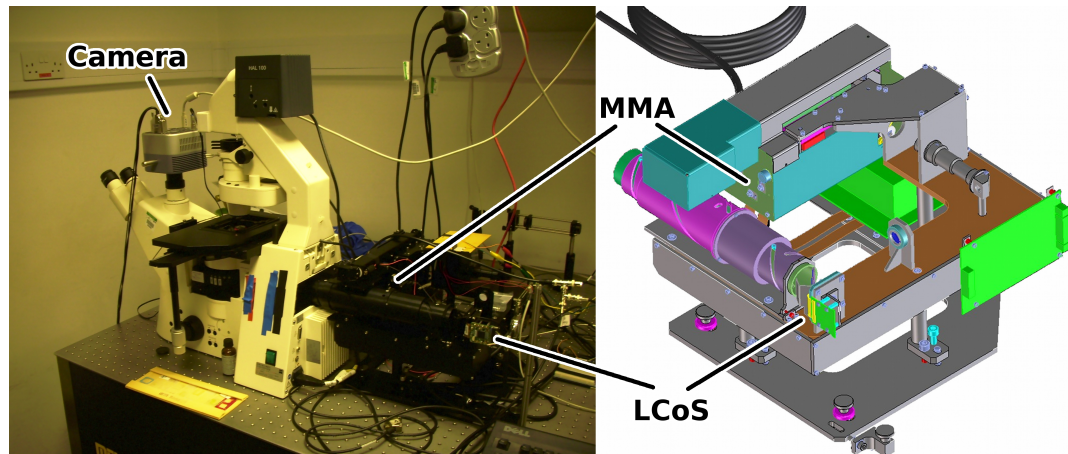

Figure 4.3: The wide field epi-fluorescence microscope with attached illumination head. The positions of the two spatial light modulators (pupil plane SLM: micromirror array (MMA) and focal plane SLM: liquid crystal on silicon display (LCoS)) are indicated. Drawing by Josef Wenisch (In-Vision, Austria).

etup-photo-blueprint⟩?

4.1.5 Thoughts about the etendue

4.1.6 Variable telescope as tube lens

Microscope objectives come with various pupil diameters. The last lens TL_{ill} in our illumination system has been designed as a variable zoom objective, that maps the pupil plane SLM from P″ with variable magnification to P.

Unlike conventional zoom telescopes we use three movable lens groups to guarantee that the image of the pupil plane SLM remains stationary and simultaneously focal plane SLM stays imaged into infinity while changing the magnification.

– email mit erhard ipp – Du gehst jetzt also mit linear polarisiertem Laser direkt in den Lichtmischtunnel? – Ja. Der Laser wird an zwei Metall-Spiegeln
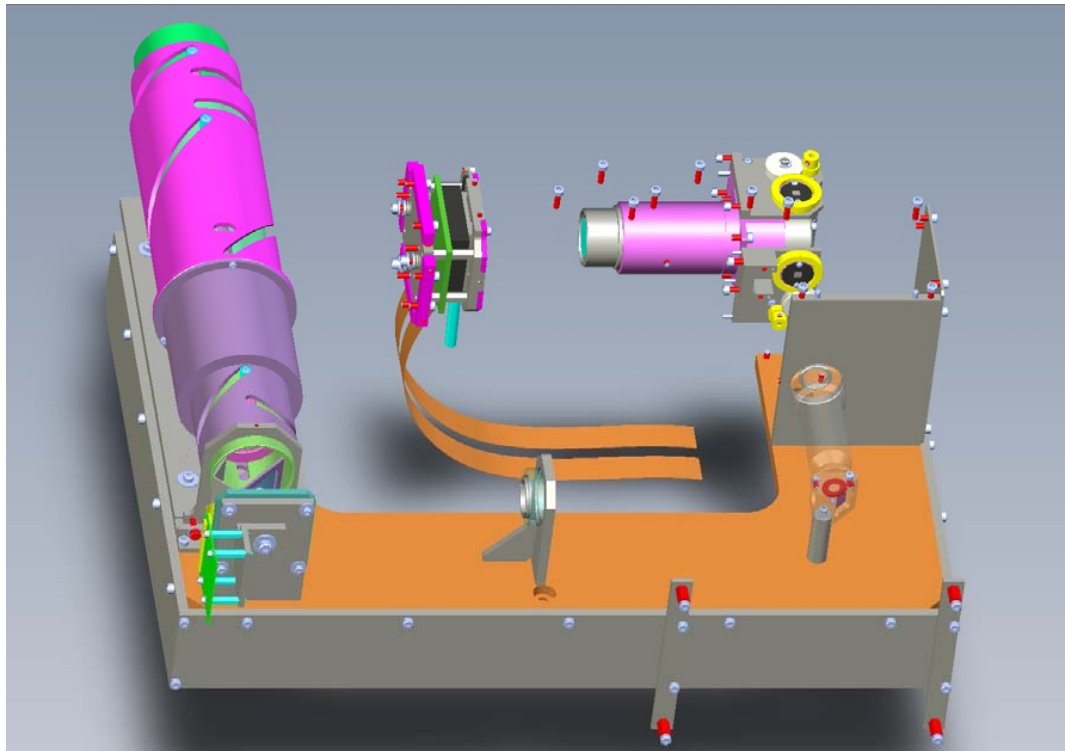
Figure 4.4: only lenses7

mi-setup-only-lenses)?

M1 und M2) reflektiert. Vor dem Mikrolinsenarray messe ich - (1.885+/-0.005) mW ohne Polarisator, (1.580+/-0.001) mW mit Polarisator in Maximalstellung und - (27.26+/-0.01) uW mit Polarisator in Minimumstellung. Der Kontrast ist 1.8e-3/27e-6=70:1.

4.2 Electronic control of the component

Both spatial light modulators can run at most with 50% duty cycle. Therefore it is necessary to synchronize the displays. Their controllers allow to upload several hundred frames of image data before an experiment and keep them in local storage. Images can then be selected by fast function calls over USB (LCoS) or Ethernet (MMA).

The camera (Clara, Andor PLC, Belfast, Northern Ireland) as the slowest device is chosen as the master. The camera provides two TTL outputs. The output "fire" is high while the camera is integrating. The output "shutter" goes high 1 ms before "fire" and provides enough time ($> 850\,\mu s$) for the MMA controller to tilt and let the mirrors settle.

The LCoS controller can display its images only for certain discrete times

(20 ms, 10 ms, 5 ms, 200 μs) and it is not straight forward to change this via USB interface. Therefore we always work with a fixed LCoS display time of 20 ms. The "fire" output of the camera also switches the laser on using an acousto-optic modulator (AOM).

When the z-stage is used, the camera is stopped until the stage has reached its target position.

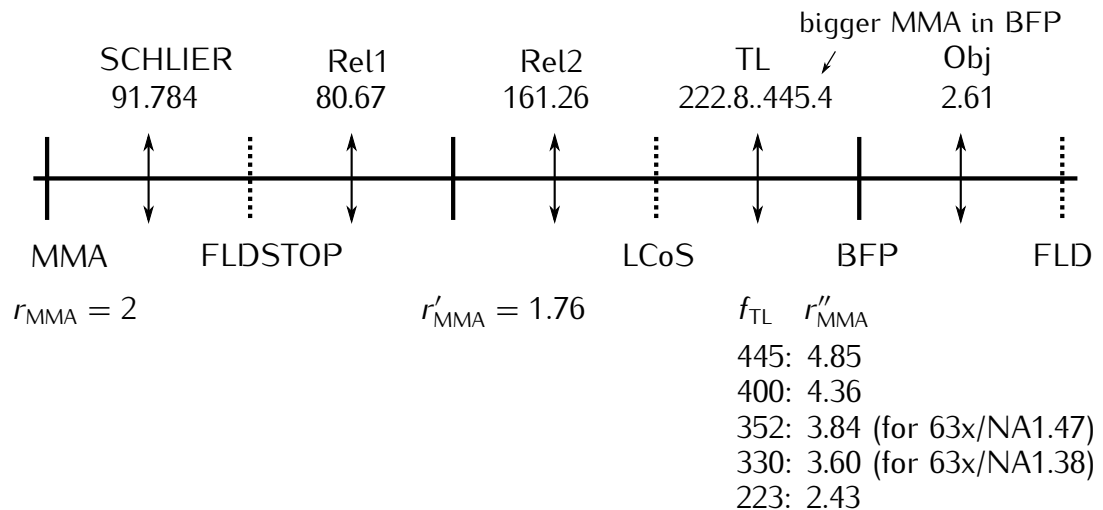(FIXME bring both these images into the appendix)

Figure 4.5: Schematic of the lenses in the MEMI system and their focal lengths. The focal length f_{TL} of the tube lens can be varied. This allows to scale the second intermediate image r''_{MMA} of the micro mirror array to fit the back focal plane of different objectives. Dimensions in mm.

?⟨fig:memi-sketch⟩?

5 optimization of the spatio-angular illumination patterns

?⟨sec:optimization⟩?

6 mma as an intensity modulator

⟨sec:mma⟩

7 experimental results with spatio-angular microscope (device 1)

?⟨sec:results⟩?

8 discussion

– zuerst habe ich dvi lcos mit mma verbaut, das hat leider nur gelegntlich funktioniert

- urspruenglich war geplant folgendes system einzusetzen: Biological applications of an LCoS-based programmable array microscope (PAM)

- dann habe ich usb lcos eingesetzt, damit geht es immer, ist aber langsamer und deutlich weniger nuetzlich zum experimentieren

- ausserdem ist die ettendue des beleuchtungssystems arg eingeschraenkt mit einem 63x objektiv (NA=1.47) wird nur ein feld mit 40 um durchmesser beleuchtet

- deshalb untersuchten wir einen anderen weg zur kontrasterzeugung und lernten dabei dass ein interferometrischer ansatz sehr wohl geeignet ist, die ettendue zu erhoehen

- einschraenkungen in der realisierbaren optik (freier durchmesser der nomarski prismen) fuehrte zu nicht ganz ueberzeugenden bildern

- ein piston mma wuerde zu deutlich besseren ergebnisse fuehren

- ein weiterer ansatz fuer spatio-angular beleuchtung wurde mit einer holographischen methode verfolgt

- dabei lernten wir dass die qualitaet des verwendeten phasenmodulators zu wuenschen uebrig laesst

- einfacherer ansatz mit nur einem display, erfordert daher weniger optik und elektronik

- loest jedoch nicht das problem geringer ettendue (die moegliche ettendue muss ich mir genauer ueberlegen, sie haengt mit der anzahl der pixel des displays und den grating konstanten zusammen, die dargestellt werden koennen, da das system off-axis betrieben werden muss, wird die ettendue geviertelt)

- Im Nachhinein muss man sagen, dass es Zielfuehrender gewesen waere, und unsere Aufgabe erheblich vereinfacht haette, wenn wir beide SLM vom gleichen Typ verwendet haetten. Es handelte sich aber um einen Prototypen und er war in den ersten Jahr des Projektes noch nicht verfuegbar. Das Projekt wird von Pasteur und Fraunhofer, diesmal unter Verwendung zweier ihrere SLM, weitergefuehrt.

– Leider wird dieser Ansatz unsereserachtens nicht das wesentliche Problem der kleinen Ettendue bereinigen und der neue Prototyp wird noch immer nicht die interessantesten Experimente erlauben. Es ist ganz einfach so, dass es einfacher waere, ein biologisch Relevantes Experiment zu designen, wenn das Beleuchtungssystem auch die volle Ettendue heutiger Mikroskopobjektive ausschoepft.

– kameras sind zur zeit an einem wendepunkt. vermutlich wuerde man heutzutage eine sCMOS benutzen, dann sollte man aber auf die triggereigenschaften achten

– arduino war nuetzlich um die elektronische triggerung ohne grossen aufwand umzusetzen (der hauptaufwand war oft nicht die zeitsteuerung, sondern eine ordentliche galvanische entkopplung der displays, die ist auch wichtig)

– da unterscheiden sich die hersteller ohnehin sehr stark, bei dem dvi display war es erforderlich, testpunkte vom board abzugreifen und ueber adum zu entkoppeln, bei neueren varianten des usb boards kann man mittlerweile einfach einen stecker anstecken

– man kann relativ viel aufwand bei der rekonstruktion von optisch geschnittenen bildern betreiben, fuer das reale problem ist die vermeidung von artefakten dann oft doch nicht so wichtig (z.b. beads oder nuklei lokalisieren)

– transmission ist nicht ausreichend um wuermer zu untersuchen

– vergleiche die folgenden displays:

– holoeye (erwaehne triggerversuche, kalibrationsmessungen von uebertragungsfunktion und interpixel cross talk, hamamatsu)

– forthdd (frage sie vielleicht, ob sie mir im nachhinein doch noch information geben)

– ti dmd (sehr gute dokumentation, sehr viele funktionen; gut waere, wenn ich ein programm auf dem lokalen arm prozessor laufen lassen koennte, was die vollen 4000fps aus runlength (oder irgendwie komprimierten) daten vom usb aus erzeugen koennte

– deflection angle defines f/# number of projection lens and therefore etendue, for good contrast f/# shouldn't be smaller than f/2.8

– mma (naja)

– hilo ist nicht unbedingt notwendig, ziemlich kompliziert und brauch fudge factor

– high density fluorophore labelling for the shorter wavelength fluorophore (better signal noise)

9 outlook

– den algorithmus zur beleuchtungsoptimierung kann man noch deutlich verbessern

– gleichzeitige beleuchtung mehrerer nuklei

– andere objektstrukturen (z.b. zylinder, axone)

– 2010 hermann cuntz: One Rule to Grow Them All: A General Theory of Neuronal Branching and Its Practical Application

– modell wie neuronen wachsen um axon oder dendritendichte vorherzusagen

– voxels05_final

– eine genaue analyse einiger probleme mit wellenoptischer partiell kohaerenter theorie steht noch aus und waere interessant (nach wichtigkeit)

– partiell kohaerente simulation des mma im schlierenoptischen system

– sind graulevel vorteilhaft?

– wuerde ein mma, bei dem alle spiegel in dieselbe richtung kippen die ettendue verdoppeln?

– partiell kohaerente simulation des mma im shearing interferometrischen system

– was ist die maximale ettendue eines wollaston prismas?

– holographie methode mit extended source

– Denkbar waere auch ein scannendes konfokales Mikroskop, dass an die Beleuchtungswinkel an jedem Punkt kontrolliert (siehe fig:hourglass-all-b). Bisher wurden in der Literatur nur Systeme beschrieben, die die Phase des Beleuchtungslicht in der Pupille aendern (FIXME ref). Eine Adaption dieser Systeme zu einem spatio-angularen ist naheliegend und ich schlage vor, derartige Systeme auch untersucht werden sollten. Die Kombination von CLEM, einem Ringdetektor (vielleicht mit UZI) koennte die Bildgebung im Inneren lebender Organe (z.B. Gehirn) verbessern.